RESEARCH ARTICLE

Design and Validation of an IMU Based Full Hand Kinematic Measurement System

PRAJWAL SHENOY [1,2], **ANURAG GUPTA** [1], **AND VARADHAN S.K.M.** [1]

[1]Department of Applied Mechanics, Indian Institute of Technology, Madras, Chennai, Tamil Nadu 600036, India
[2]Department of Mechatronics Engineering, Manipal Institute of Technology, Manipal Academy of Higher Education, Manipal, Karnataka 576104, India

Corresponding author: Varadhan S.K.M. (skm@iitm.ac.in)

ABSTRACT Measurement of hand kinematics is commonly done using data gloves and optical trackers and finds application in biomechanics, motor control research, clinical assessment, virtual reality etc. While data gloves are expensive and restrict the dexterity of the hand, optical trackers are susceptible to the line-of-sight problem and can be used only in a laboratory setting. Over the last decade, the use of Inertial Measurement Units (IMUs) to measure kinematics has gained traction due to their affordability and good accuracy. This paper presents the design and validation of a BNO055 IMU-based full Hand Kinematics Measurement System (HKMS). The best features from existing IMU-based devices were identified from the literature and incorporated. The HKMS streams orientation information of 16 BNO055 IMUs in real-time at 100 Hz via Wi-Fi or USB. A rigorous static and dynamic validation of the BNO055 IMU was done against 3D printed models and the highly accurate Electro Magnetic Tracking System (EMTS). The RMSE errors were found to be acceptable for the measurement of hand kinematics. Two experiments were conducted to collect hand kinematic data for various postures and object grasps using the HKMS and EMTS, respectively. Synergy analysis was done and range of motion of the joints was calculated using the two datasets. The results were compared to get an idea of the quality of the dataset collected using the HKMS. The results as well as the overall validation of the sensors indicate that the HKMS may be suitable for usage in a laboratory or clinical setup.

INDEX TERMS BNO055, data gloves, hand kinematics, IMU, IMU validation, inertial measurement unit, joint angles, motion capture, synergy.

I. INTRODUCTION

The human hand is the epitome of dexterity and fine movement control. With monosynaptic connections between the cortico-spinal neurons and the alpha motor neurons supplying the hand muscles, the dexterity and complexity of movements of the human hand is unparalleled. While such dexterity helps us to grasp and manipulate objects with varying shapes and contours with ease, the presence of a large number of joints poses a challenge for measuring the kinematics of the

The associate editor coordinating the review of this manuscript and approving it for publication was Masood Ur-Rehman.

hand or in the design of artificial hands. Accurate measurement of human hand kinematics is essential in biomechanics, motor control research, synergy analysis, sports, hand animation, virtual reality (VR), ergonomics etc. Apart from this, physicians also consider parameters like the range of motion (ROM) and smoothness of movements as reliable indicators to track the severity of pathology and recovery rate in patients with neuromotor disorders. Research in these areas heavily relies on devices such as optical trackers [1], [2], [3] and flex sensor-based data gloves [4], [5], [6], [7], [8] to measure full hand kinematics. Optical trackers require an external setup in terms of cameras and placement of markers

on the hand and hence cannot be used for quick measurements outside of a laboratory setup (e.g., in a clinical setup). Additionally, they are also susceptible to line-of-sight problems. Since human hand kinematic measurement requires many markers, line-of-sight problems are inevitable. Commercially available data gloves are made using multiple flex sensors whose resistance changes based on the amount of bend in them. Using appropriate calibration methods, these resistance values are converted to joint angles [9]. These calibration methods must be repeated for each participant separately due to their varying hand sizes. As a result, inaccuracies could creep into the measurements if the calibration process is not done correctly. Additionally, a recent study has shown that the dexterity of movements decreases by 29% while wearing data gloves due to the obstruction provided by the glove on the palmar surface of the hand [10]. Moreover, commercially available data gloves and optical trackers are expensive.

Over the last decade, the use of Inertial Measurement Units (IMUs) for the measurement of hand kinematics has gained serious traction due to their affordability, ruggedness, ease of use, and relatively good accuracy. Many existing IMU-based data gloves [12], [16], [17], [18], [19], [20], [21], [22], [23], [24], [25] measure rudimentary quantities such as acceleration, tilt rate and magnetic field using the IMUs accelerometer, gyroscope and magnetometer, respectively. These quantities are then processed using sensor fusion algorithms that use appropriate filters to obtain the orientation of the IMU sensor and, in turn, the orientation of the finger phalanx to which the IMU is attached to. This orientation is obtained w.r.t the north east down (NED) or east north up (ENU) reference frame. The orientation data is in turn used to compute joint angles. Of late, a few IMUs such as the BNO055 (by Bosch Sensortec), BNO080/85/86 (co-developed by Hillcrest Labs and Bosch Sensortec), MPU9250 (by InvenSense) etc., have gained immense popularity amongst hobbyists and researchers alike [11], [12]. This is due to the fact that they have an onboard microcontroller (integrated into the IMUs System in Package (SiP)) that implements a sensor fusion algorithm to output orientation data (in the form of quaternions and/or Euler angles) in real-time at sampling rates as high as 100 Hz. (For e.g., the BNO055 IMU has a 32-bit microcontroller (as part of the IMU chip) which implements a Kalman filter-based sensor fusion algorithm to output orientation data (as quaternions or Euler angles) at 100 Hz). This has been a real game-changer as these IMUs are now accessible to those audiences who might not necessarily have an intimate knowledge of signal processing techniques and complex filters required for implementing the sensor fusion algorithm in real-time.

In this paper, we present the design and validation of a BNO055 IMU-based Hand Kinematics Measurement System (HKMS) with Wi-Fi capability for the measurement of full hand kinematics (15 joints). The utility of the HKMS in collecting hand kinematic data for ROM analysis and synergy analysis is also demonstrated. In the following section, existing IMU-based data gloves are compared and contrasted from the literature and some limitations are identified. Based on the limitations, the important factors that should go into the development of the HKMS are highlighted.

II. RELATED WORK

The last decade has witnessed tremendous growth in the development of IMU-based devices for tracking human hand movement. Many of these devices have reported relatively good accuracy without hindering natural hand movements and object manipulation. Some of these devices have been developed to measure full hand kinematics (Refer Table 1), whereas others have been developed specifically for certain applications and don't measure the kinematics of all the finger joints [13], [14]. In this paper, only the literature pertaining to IMU-based devices that measure full hand kinematics is discussed.

A list of IMU-based data gloves/systems for the measurement of full hand kinematics is presented in Table 1. Some of the crucial aspects of the data gloves, such as the IMU used, sensor size, data output rate, ability to implement the sensor fusion algorithm in real time and location of implementation of the algorithm (i.e., on PC, on microcontroller or on board the IMU chip itself), validation methods, and mode of data transfer are compared in Table 1. From the table, it can be seen that IMUs like MPU9250, MPU9259, MPU6050, BNO055 and LSM series are some of the commonly used sensors for the development of IMU-based data gloves. Recently, a preliminary study investigated the static and dynamic accuracy of three consumer-grade IMUs: MPU9150, X-NUCLEO_IKS01A1, BNO055 and one industrial-grade IMU: MTi-300 [15]. The results showed that among the consumer-grade IMUs, the BNO055 had better static and dynamic accuracy. This was one of the reasons why we explored the possibility of using the BNO055 in building the HKMS.

From the literature (Refer Table 1) the following drawbacks of existing IMU-based data gloves have been identified:

1. IMU data gloves that use USB [11], [12], [16], [24] to output data limit the movement range of the glove to the length of the USB cable. While there are IMU data gloves that use Bluetooth (Refer Table 1) for wireless data transmission (hence overcoming the limitation), using Wi-Fi would give superior range and data transmission speeds.

2. Many IMU data gloves output orientation data at low sampling rates, e.g., 20Hz [11], 50 Hz [18], 60 Hz [21] etc. Some IMU data gloves output raw data at sampling rates of 50 Hz [17], [20], [23], [25], 100 Hz [12], [16], [22] etc., and process the raw data using sensor fusion algorithms to get orientation data in real time. However, some of these studies have not clearly stated what is the orientation data output rate after processing the raw data. Existing, commercially available flex-sensor based data gloves output joint angle information at 100 Hz or greater [8], [26]; hence it would be desirable to make the HKMS output orientation data at 100 Hz to meet the commercially available standards.

TABLE 1. Comparison of IMU based full hand kinematic measurement devices.

Study Ref No (Year)	IMU used (Dimensions in mm)	Number of IMU's	Data Output Rate (Raw /Orientation Data)	Sensor Fusion Algorithm (Implementation location)	Validation	Validation device	Static RMSE /error	Dynamic RMSE /error	Wi-Fi /BT/USB
[16] (2014)	ST LSM330DLC (unspecified)	16	100 Hz (Raw data)	Real time (PC)	Dynamic	Optical tracker	-	1.2 cm	USB
[17] (2017)	MPU6050 (unspecified)	11	50 Hz (Raw data)	Real time (PC)	Dynamic	Optical tracker	-	3.3°	BT
[18] (2017)	MPU9250 (10 x 15 x 2.6)	18	50 Hz (Orientation data)	Real time (Microcontroller)	Static and dynamic	Robotic arm	< 1°	2.5°	BT
[11] (2017)	BNO055 (6.35 x 6.35)	15	20 Hz (Orientation data)	Real time (On-Board the IMU)	Static and dynamic	3D printed/ motorized platform	8° (Max error)	6° (Max error)	USB
[19] (2017)	MPU9150 (unspecified)	16	Unspecified	Real time (PC)	Static	Wooden cuts and optical tracker	5.95°	-	Wi-Fi
[20] (2018)	LSM9DS0 (10 x 10)	17	50 Hz (Raw data)	Real time (PC)	Static and dynamic	LPMS-B IMU	1°	2.3°	BT
[21] (2018)	Unspecified (Unspecified)	17	60 Hz (Orientation data)	Real time (Microcontroller)	Dynamic	4 d.o.f gimbal	-	5.7°	BT
[22] (2019)	MPU9259 (unspecified)	16	100 Hz (Raw data)	Real time (PC)	Dynamic	Optical tracker	-	2cm	BT
[23] (2019)	Unspecified (unspecified)	16	50 Hz (Raw Data)	Unspecified	Static	Protractor tool	2°	-	BT
[24] (2019)	Unspecified (12 x 8)	16	Unspecified	Real time (Microcontroller)	Dynamic	Custom motorized platform	-	3°	USB
[25] (2019)	MPU9250 (unspecified)	18	50 Hz (Raw Data)	Real time (PC)	Dynamic	Optical tracker	-	5°	BT
[12] (2021)	MPU9250 (unspecified)	12	100 Hz (Raw data)	Real time (PC)	Static and dynamic	Goniometer and HCM365B compass	<2°	Not reported	USB
This device HKMS	**BNO055 (10 x 13)**	**16**	**100 Hz (Orientation data)**	**Real time (On-board the IMU)**	**Static and Dynamic**	**3D printed models and EMTS**	**Details discussed in results**		**Wi-Fi and USB**

3. Most of the IMU data gloves process the raw data using sensor fusion algorithms to get orientation data. However, to reproduce such devices would require advanced knowledge of signal processing techniques and complex filters (which is required to implement the sensor fusion algorithm). With recent advances in technology, IMU's such as the BNO055 have emerged which directly output orientation data at 100 Hz. This eliminates the requirement of the end user to implement a sensor fusion algorithm. Using such an IMU to develop the HKMS would greatly reduce the complexity,

the device development time and make the HKMS easier to reproduce in comparison with existing IMU data gloves.

4. An essential aspect of any IMU-based data glove/system is the validation process wherein the sensor outputs are benchmarked against a highly accurate system. Optical trackers [16], [17], [22], [25], high accuracy laboratory-grade IMUs [20], and custom-made motorized platforms [11], [21], [24] are some of the commonly employed devices for validation. While these validation methods have reported high accuracy in favor of the IMU-based data gloves, liter-

ature reporting a detailed and rigorous static and dynamic validation (involving the effect of different movement speeds and continuous repetitive movements on the IMUs accuracy) is scarce.

5. Finally, studies that have demonstrated an application of the developed IMU-based data glove [19] in a laboratory or clinical setup are scarce.

From the discussion in the preceding paragraphs, we have identified the following important factors that should go into the development of an IMU-based data glove/system: use of 16 IMUs to measure full hand kinematics, minimum strapping on the palmar surface of the hand to prevent reduction in hand dexterity, outputting the orientation data (in the form of quaternions) of all the 16 IMUs at 100 Hz, using an IMU that has a microcontroller (onboard the IMU chip) which implements a sensor fusion algorithm to directly output orientation data in real-time, rigorous static and dynamic validation of the chosen IMU and wireless data transmission using Wi-Fi. We have built a BNO055 IMU-based Hand Kinematics Measurement System (HKMS) that incorporates all these factors.

Apart from design and validation of the IMUs, as an application of the HKMS, we test its utility in the measurement of ROMs and analysis of synergies derived from the measured kinematics. According to human motor control research, a small number of movement primitives (also called synergies) are capable of controlling a larger set of joint movements of the human hand, resulting in simultaneous activation of multiple joints [4]. Instead of individually controlling each degree of freedom of the hand, the central nervous system (CNS) relies on such synergies or coactivation patterns to control the complex set of hand movements, hence reducing its computational load. Dimensionality reduction using PCA [1], [2], [3], [4], [5], or autoencoders [8], are usually applied to identify the synergistic kinematic patterns which could help in disease diagnostics [26] or development of prosthetic hands [27], [28]. We conducted an experiment where the HKMS was used to collect kinematic data (from 5 participants), which in turn was used for synergy analysis and ROM analysis. The same experiment was conducted again (with the same 5 participants), but instead of using the HKMS, a highly accurate Electromagnetic Tracking System (EMTS) was used for kinematic data collection. The kinematic synergy patterns and ROM derived from the HKMS were compared with that obtained from EMTS. This was done to get a sense of how the HKMS compares to highly accurate research-grade equipment in terms of the quality of the data set collected and its use in reproducing similar results and interpretations. In this paper, we present:

1. The design of the BNO055 based HKMS,

2. The static validation of the BNO055 IMUs against 3D printed models with predefined joint angles,

3. The dynamic validation of the BNO055 IMUs against the highly accurate EMTS sensors and

4. The experimental results of synergy analysis and ROM analysis of two separate data sets collected using the HKMS and the EMTS, respectively.

III. MATERIALS AND METHODS
A. HARDWARE DESIGN
The HKMS consists of 6 microcontrollers and 16 IMU sensors. One microcontroller is a Wi-Fi module which is used to wirelessly send data from the HKMS to the computer via Wi-Fi. The remaining 5 microcontrollers are used to collect orientation data in the form of quaternions from the 16 IMUs. These 5 microcontrollers are connected in a master slave configuration: 1 master and 4 slaves (See Fig. 1(b)). The master is connected to 4 IMU's – 1 placed on the wrist and 3 placed on the phalanges of the middle finger. Each of the 4 slaves are connected to 3 IMUs which are placed on the three phalanges of a finger (See Fig. 1(b)). The data collection is synchronized by the master in the following way: the master sends an interrupt (in the form of a rising edge on the interrupt line) to the 4 slaves every 10ms. Upon detecting the interrupt, the 4 slaves simultaneously start collecting orientation data from the three IMUs connected to them. Each slave then sends the collected data serially to the master. Parallelly, the master, after generating the interrupt, starts collecting orientation data from the 4 IMUs connected to it following which it waits for the serial data to arrive from the 4 slaves. Once all the data has arrived, the master sends the data serially to the Wi-Fi module which in turn wirelessly sends the data to a computer. Alternatively, the master can also send the data via USB to a computer. This entire process of collecting and sending the orientation data from all the 16 IMUs happens within 10ms before the master sends the next interrupt. This ensures that the HKMS outputs the orientation data at a frequency of 100 Hz.

One of the unique design features of the HKMS is the master-slave configuration explained in the preceding paragraph. The reason for using such a design is the following: the IMU being used in the HKMS takes approximately 2-3ms to send the orientation data to the microcontroller from the instance at which the IMU was requested for the data. If a single microcontroller is used, then it would take $\geq$32ms to get data from all the 16 IMUs. This would limit the sampling frequency of the HKMS to $\leq$31.25 Hz. However, as discussed in the previous section, it was decided that one of the features of the HKMS should be that it outputs orientation data from all the 16 IMUs at 100 Hz. To achieve this, the master-slave configuration was used to enable simultaneous data collection from multiple IMUs and hence, achieve the desired sampling rate of 100 Hz. Additionally, the number of IMUs on the HKMS can be expanded to 20 without decreasing the 100 Hz sampling rate. These additional sensors can be placed on the wrist to model the palm arch of the hand or on the arms to capture their movement kinematics. Another unique design feature of the HKMS is connecting the IMU sensors in series.
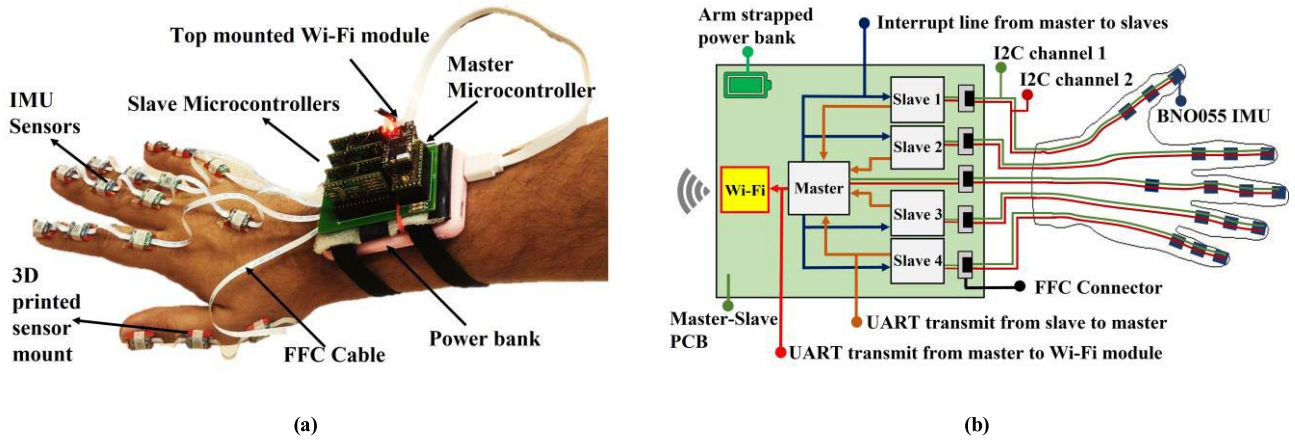
FIGURE 1. (a) The HKMS is mounted on a human hand. The IMU's are stuck to the finger phalanges and the Master-Slave receiver board is strapped to the arm along with a power bank (b) Simplified block diagram of the HKMS showing the connections between the master microcontroller, slave microcontrollers, BNO055 IMUs and the Wi-Fi module. The serial communication protocol between the master and slaves is UART and between the BNO055 IMUs and the microcontrollers is I2C.

This was done to reduce the bulkiness of the device. Instead of having individual connections to each of the 16 IMUs, the 3 IMUs connected to each slave were connected in series and the 4 IMUs connected to the master were connected in series (See Fig. 1). To achieve the series connection, four different "types" of Printed Circuit Boards (PCBs) were designed around the IMU chip. The design and implementation details of these four "types" of PCB's are provided in Appendix I.

B. HARDWARE IMPLEMENTATION

The HKMS consist of 5 teensy 4.0 microcontrollers used in the master-slave configuration, an ESP32 based microcontroller – TinyPICO – having Wi-Fi capability for wireless data transmission, 16 BNO055 IMUs (Bosch Sensortec) for providing orientation information of the wrist and all the finger phalanges and a small power bank for powering the HKMS (See Fig. 1(a)). In order to build a compact system, a custom PCB – Master-Slave PCB – was designed with appropriate connections between the master and slaves (See Fig. 1(b)). This PCB has dimensions of 7.3 cm x 5 cm, consists of slots for fixing the 5 teensies and has 5 Flat Flexible Cable (FFC) connectors soldered at the bottom. The Master-Slave PCB is strapped to the arm along with the power bank using Velcro straps (See Fig. 1(a)). It is not attached to the wrist so as to avoid any strapping material on the palmar surface of the hand which could reduce the hand's dexterity. The serial communication between the master, slaves and the TinyPICO (which is directly soldered on top of the master) happens using the UART communication protocol and the serial communication between the BNO055s and the teensies happens using the I2C communication protocol. The FFC connectors on this PCB are 6 pin 0.5mm pitch connectors. Two pins of the FFC connector are dedicated for the power lines and the remaining four pins are dedicated for connections to two I2C channels (shown in Fig. 1(b) as I2C channel 1 and I2C channel 2) of a single teensy. Each FFC connector on this

PCB connects one teensy to the three BNO055 sensors on one finger. The three BNO055s on each finger are connected in series using 6 wire FFC cables (0.5 mm pitch). For the master alone, 4 BNO055s are connected in series (See Fig 1). To connect the BNO055 sensors in series and to minimize its size so that it can be attached on a finger phalanx, four different "types" of custom PCBs having a dimension of 1.3 cm x 1 cm were designed around the BNO055 chip. The design of these four "types" of PCBs and how they are connected in series is given in Appendix I.

C. QUATERNION PROCESSING AND ANIMATION OF HAND MODEL

The BNO055 IMUs were programmed to output orientation data in the form of quaternions. As a first step in processing the data, the relative quaternions between the adjacent BNO055s across all joints were computed using quaternion conjugate multiplication (1).

$$q_{BrelativeA} = q_A{}^{conj} \otimes q_B \qquad (1)$$

Here, q_A and q_B are the raw quaternion data of the two adjacent hand segments 'A' and 'B' of a joint and represents the orientation of these segments w.r.t east north up (ENU) frame of reference, $q_A{}^{conj}$ is the conjugate of $\mathbf{q}_A$ and $q_{BrelativeA}$ is the relative quaternion that represents the orientation of segment B relative to A. The relative quaternions of each joint were then hemispherized (i.e., made to lie on the same side of the hemisphere) due to their antipodal symmetry. The hemispherized relative quaternions were then used for data analysis.

In this work, many linear Euclidian operations such as computing RMSE, performing linear dimensionality reduction using PCA etc., are performed. However, since quaternions are defined on a non-linear manifold, the linear operations just mentioned cannot be directly applied on them [29], [31]. To perform these linear operations, the
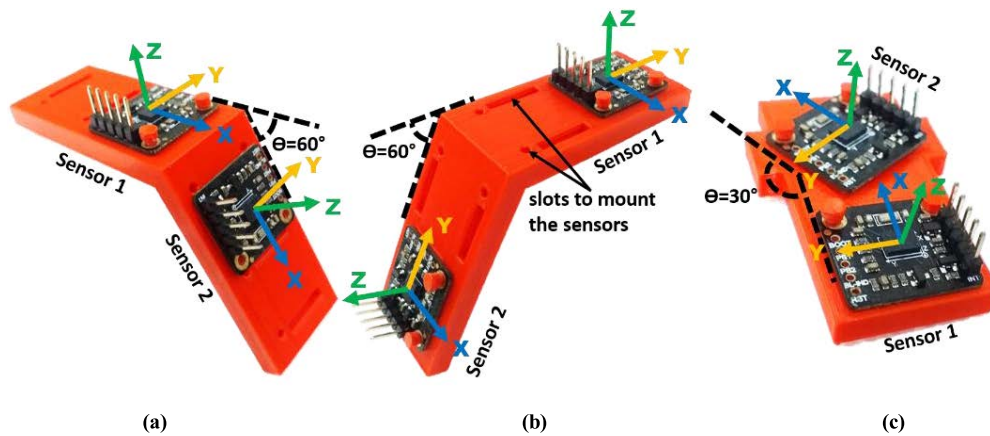
FIGURE 2. 3D printed models (used for static validation) with slots to mount the BNO055 breakout boards at fixed angles relative to each other. The local reference frame of each BNO055 sensor is highlighted. (a) and (b) depict the same 3D printed model having a joint angle of $\theta = 60°$. In (a), the sensors are fixed such that sensor 2 is rotated 60° w.r.t the Y axis of sensor 1 i.e., the relative pitch angle is 60°. In (b), the sensors are fixed such that sensor 2 is rotated 60° w.r.t the X axis of sensor 1 i.e., the relative roll angle is 60°. In (c), the 3D printed model has slots such that sensor 2 is rotated by 30° w.r.t the Z axis of sensor 1 i.e., the relative yaw angle is 30°.

hemispherized relative quaternions were first linearized using logarithmic mapping and then the linear operations were performed on them. Following this step, the linearized orientations were converted back to quaternions using exponential mapping [31]. For more details on the applicability of quaternions for biomechanical analysis, refer to [29], and for more information on logarithmic and exponential mapping, refer to [30], [31]. A short primer on logarithmic and exponential maps is presented in Appendix II.

For the purposes of animation, a hand model was created using SOLIDWORKS and imported into MATLAB. A MATLAB Simulink program was developed to accept the orientation data from the HKMS via Wi-Fi in real-time. Relative quaternions were computed using (1) and converted to Euler angles for the "XZY" intrinsic rotation sequence to get the roll, yaw and pitch angles of B w.r.t A. The MATLAB function 'eulerd' with 'point' as the rotation type was used for the same. The sensors were aligned on the hand such that the yaw angle (i.e., second Euler angle in the intrinsic sequence) of the proximal phalanx of a finger, when computed w.r.t the wrist sensor gave the abduction/adduction angles of that finger w.r.t the wrist sensor. The problem of gimbal lock (often encountered when working with Euler angles) is avoided in our application as the abduction angle never approaches $\pm 90°$. The computed Euler angles were then fed into the hand model to animate hand postures in real-time.
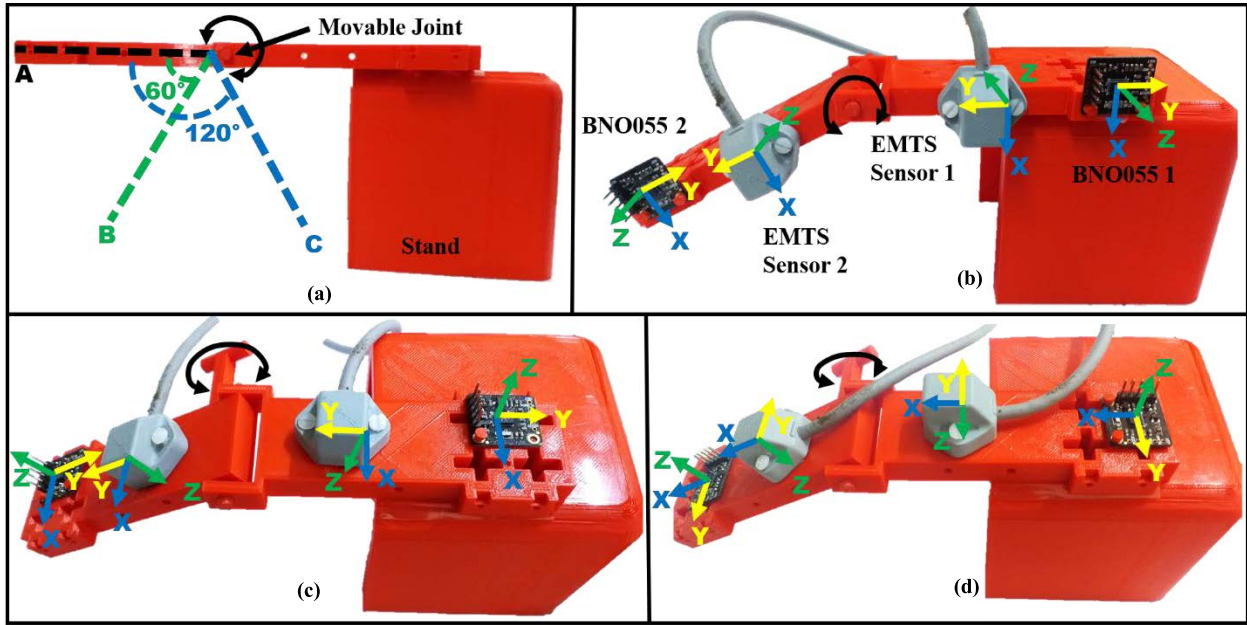
D. STATIC AND DYNAMIC VALIDATION OF THE BNO055 SENSORS

The static and dynamic validation of the BNO055 sensors was done to determine the accuracy of the BNO055 for the calculation of joint angles. This validation was necessary to determine whether the BNO055 could be used to collect full hand kinematics data for research purposes. For the static and dynamic validation, two off-the-shelf BNO055

breakout boards from DFRobot were used. Additionally, for the dynamic validation, an electromagnetic tracking system (EMTS) – Polhemus Liberty^{TM} 240/16 – was used. Two sensors were connected to the EMTS to acquire the orientation data w.r.t the reference frame of the EMTS source box kept nearby.

1) STATIC VALIDATION

For the static validation, eight 3D models with slots and holes to mount two BNO055 breakout boards were designed using SOLIDWORKS and 3D printed (Fig. 2 depicts two such 3D models). These 3D models had slots such that upon fixing the BNO055 sensors on them, the relative (pitch, yaw, roll) Euler angles of sensor 2 w.r.t sensor 1 could be set at the following 12 options: (30°, 0°, 0°), (60°, 0°, 0°), (90°, 0°, 0°), (120°, 0°, 0°), (0°, 0°, 30°), (0°, 0°, 60°), (0°, 0°, 90°), (0°, 0°, 120°), (0°, 15°, 0°), (0°, 30°, 0°), (0°, 45°, 0°) and (0°, 60°, 0°). These angles were chosen keeping in mind the ROM of the finger joints. The following protocol was followed for the static validation of the sensors: For each of the 12 options, 10 trials (10 × 12=120 trials) of sensor data was collected. Each trial lasted for 10s. A TEENSY 4.0 microcontroller collected the orientation data from the two BNO055s in the form of quaternions at 100Hz and sent this data serially to a computer. The computer had a custom LabVIEW program running which accepted and stored the incoming serial data from the microcontroller. Before the start of each trial, the orientation of the 3D model was changed, but during the trial itself, the 3D model was stationary. This was done (i.e., changing orientation before each trial) to assess the sensor's accuracy when they were at different orientations w.r.t the magnetic north and earths gravitational field. Additionally, it was also ensured that no metallic device was kept at least 5ft from the 3D model to avoid any magnetic interference in the magnetometer of the BNO055 IMUs.

FIGURE 3. 3D printed model (used for dynamic validation) with slots to attach the BNO055 and EMTS sensors at different orientations. (a) Side view of the model. The rotation of the movable segment for condition 1 is between A and B and for conditions 2 and 3 is between A and C. (b) The sensors are fixed such that the BNO055 2 and EMTS sensor 2 will rotate w.r.t the Z axis of BNO055 1 and EMTS sensor 1 respectively (i.e., change in the relative yaw angle). (c) The sensors are fixed such that the BNO055 2 and EMTS sensor 2 will rotate w.r.t the X axis of BNO055 1 and EMTS sensor 1 respectively (i.e., change in the relative roll angle). (d) The sensors are fixed such that the BNO055 2 and EMTS sensor 2 will rotate w.r.t the Y axis of BNO055 1 and EMTS sensor 1 respectively (i.e., change in the relative pitch angle).

For determining the accuracy of the sensors, the relative quaternion between the two sensors was computed using (1). The relative quaternion was then converted to Euler angles, as mentioned in the previous section. The computed Euler angles were then compared with the corresponding fixed angle of the 3D printed model. For each of the 12 options, the maximum, minimum and average of the three Euler angles across the 10 trials were computed. The error was then calculated by computing the mod of the difference between the averaged Euler angles from the expected/set Euler angles using eq (2).

$$
\begin{bmatrix} \delta_x \\ \delta_y \\ \delta_z \end{bmatrix} = \left| \begin{bmatrix} E_x^{set} \\ E_y^{set} \\ E_z^{set} \end{bmatrix} - \begin{bmatrix} E_x^{average} \\ E_y^{average} \\ E_z^{average} \end{bmatrix} \right| \quad (2)
$$

Here, δ is the error, E is the Euler angle, the subscripts x, y and z of E indicate that the Euler angle is pitch, yaw and roll respectively. While such subtraction and averaging of Euler angles is not valid in most cases, in this case, the variation of the Euler angles across samples was very less as the sensors were fixed in position relative to each other. In such a case, the Euler angles can be subtracted and averaged with negligible error [29].

2) DYNAMIC VALIDATION

For the dynamic validation of the BNO055 sensors, a 3D model having two segments joined together by a 1DOF movable joint (See Fig. 3(a)) was designed using SOLIDWORKS and 3D printed. This model had slots and holes to mount

the BNO055 breakout boards and EMTS sensors at different orientations. A part of one segment of the model was firmly stuck to a 3D printed stand (See Fig. 3(a)) to keep it stationary while the other segment was being rotated about the joint. For the dynamic validation, three conditions were tested: 1. Rotation of BNO055 2 relative to only the Z-axis of BNO055 1 (See Fig. 3(b)), i.e., change in the relative yaw angle only, 2. Rotation of BNO055 2 relative to only the X-axis of BNO055 1 (See Fig. 3(c)), i.e., change in the relative roll angle only and 3. Rotation of BNO055 2 relative to the Y-axis of BNO055 1 (See Fig. 3(d)), i.e., change in the relative pitch angle only. For all the three conditions, the EMTS sensors were fixed such that EMTS sensor 2 would rotate relative to only the Z, X and Y axis of EMTS sensor 1 for conditions 1, 2 and 3, respectively (See Fig. 3). Since the local frames of the BNO055 and EMTS sensors were different (See Fig. 3), appropriate quaternion transformations were used to align the BNO055s frame with the EMTS sensors frame during postprocessing. For each condition, the movable segment of the model was manually rotated by the experimenter to the beat of a metronome. For condition 1, the segment was rotated between A and B (60°) (See Fig. 3(a)), and for conditions 2 and 3, the segment was rotated between A and C (120°) (See Fig. 3(a)). This range was selected keeping in mind the ROM of the finger joints. A smaller range was chosen for yaw rotations since the yaw (abduction/adduction) range in human fingers is less when compared to the pitch range of the finger joints and thumb roll movement range relative to the wrist. The direction of rotation was reversed at
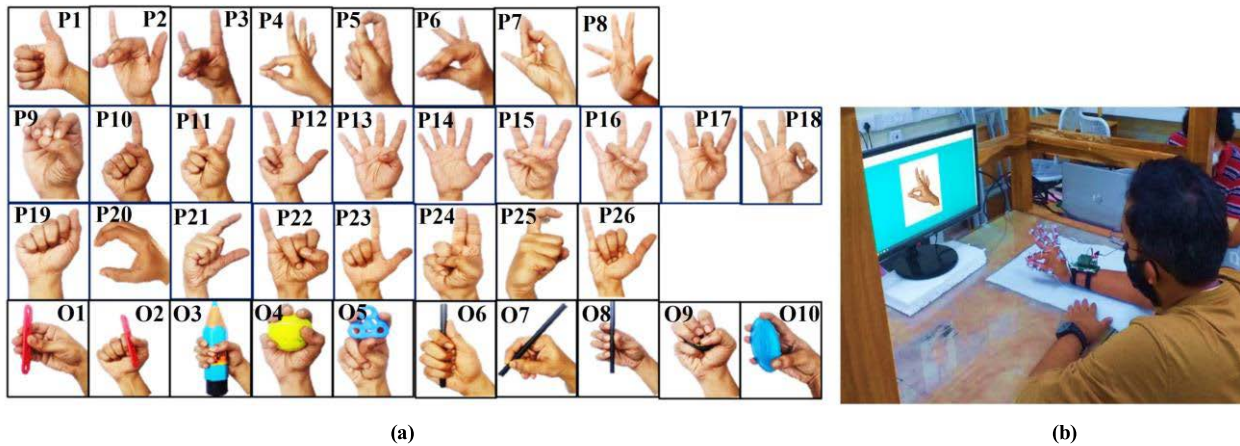
FIGURE 4. (a) Hand postures and object grasps used in the study. The participants performed 26 hand postures including Bharatanatyam dance postures (P1-P8), ASL numbers (P9-P18), ASL letters (P19-P26) and 10 object grasps (O1-O10) covering various grasp taxonomies. (b) Participant with HKMS attached to hand performing postures displayed on the screen.

the sound of each beat, and the rotation was paced such that at the time of the beat, the rotating segment was approximately at one of the following end positions: A or B for condition 1 or A or C for conditions 2 and 3.

For each condition, 40 trials of data were collected ($40 \times 3 = 120$ trials total). Each condition was in turn divided into four sub-conditions of 10 trials each. The interval between two metronome beats for the four sub-conditions was different. They were 2s, 1.5s, 1s and 0.5s, respectively. Therefore, for beat intervals of 2s, 1.5s, 1s and 0.5s, the angular velocity of the segment rotation was approximately $30°/s$, $40°/s$, $60°/s$, and $120°/s$ respectively for condition 1, and $60°/s$, $80°/s$, $120°/s$ and $240°/s$ respectively for conditions 2 and 3. Each trial lasted for 20s. The orientation data in the form of quaternions for the two EMTS sensors and the two BNO055 IMUs were streamed to a computer by the Polhemus Liberty EMTS at 240Hz and a TEENSY 4.0 microcontroller at 100Hz, respectively. A custom LabVIEW code was running on the computer, which simultaneously accepted the incoming data from both the systems. The timestamp information of the arrival of each BNO055 data frame (1 frame = one sample from both the BNO055's) and arrival of each EMTS sensor data frame was stored by the program. The two timestamps were then used in post-processing to match each frame of the BNO055 data with the nearest frame of the EMTS sensor data so that they could be compared. Additionally, the LabVIEW program also generated the metronome beat.

For determining the dynamic accuracy of the BNO055 in calculating the relative orientation of one sensor w.r.t the other, the relative quaternion between the two BNO055s and the two EMTS sensors were first computed using (1). The RMSE between the two sets of relative quaternions was then computed using (3) [31]. This particular RMSE is a single value that represents the error in degrees between the two sets

of relative quaternions.

$$(RMSE) = \sqrt{\sum_{i=1}^{n} \frac{1}{n} \|ln(Q_i^{conj} \otimes Q_e)\|^2} \qquad (3)$$

Here, Q_i and Q_e are the relative quaternions of the BNO055 and EMTS sensors, respectively. $\|ln(Q_i^{conj} \otimes Q_e)\|$ gives angle in degrees. This angle is the smallest angle required for one quaternion to rotate about an axis to reach the other quaternion.

3) CALIBRATION OF THE BNO055 SENSOR

The BNO055 IMU contains three sensors: a gyroscope, an accelerometer and a magnetometer. For the BNO055 to give accurate readings, these three sensors need to be calibrated every time the BNO055 is powered on. Each of these sensors has a value between 0 and 3 associated with it that indicates the calibration status of the sensor. If the value is 0, then the sensor is not calibrated, and if the value is 3, then it is fully calibrated. The process to calibrate these sensors are different and are specified in the following resources [32, p. 51, 35]. The BNO055 needs to be kept stationary for a few seconds to calibrate the gyroscope. The BNO055 needs to be rotated at $45°$ increments about at least one of its axes to calibrate the accelerometer. After each $45°$ increment, it needs to be kept stationary for a few seconds. This needs to be done until the calibration status of the accelerometer becomes 3. The BNO055 needs to be moved in the air for a few seconds as if drawing the infinity sign to calibrate the magnetometer. It takes approximately 30s to calibrate all three sensors.

For the static validation, the BNO055s were calibrated at power on. For each BNO055, the calibration status of the three sensors was checked between each trial. It was observed that all the calibration values remained 3 throughout all the trials. For the dynamic validation, the calibration values for

each BNO055 were monitored between trials and during the trials as well. It was observed that the magnetometer calibration value decreased during trials as well as between the trials. This can be attributed to the magnetic field emitted by the EMTS source box, which adversely affects the accuracy of the magnetometer. Whenever the calibration value of the magnetometer became 0 during the dynamic validation, it was recalibrated before proceeding with further trials.

E. EXPERIMENTAL VALIDATION OF THE HKMS ON THE HAND

In order to compare the performance of the HKMS with that of the EMTS for analyzing full hand kinematic data, two experiments were conducted. In the first experiment, 5 participants performed 26 hand postures, and 10 object grasps (See Fig. 4). 16 EMTS microsensors (different and smaller than the ones used in the dynamic validation of the BNO055) from Polhemus were used to collect full hand kinematic data. The second experiment was the same as the first one, the only difference being that the HKMS was used to collect full hand kinematic data instead of the EMTS. The participants for both the experiments were the same. Two separate experiments needed to be conducted as both the BNO055 and the EMTS sensors could not be simultaneously mounted on the finger phalanges due to lack of space. Inability to collect data simultaneously from both the EMTS and HKMS in a single experiment is a limitation in the validation step of the HKMS. Details of both the experiments are given in the following sections.

1) PARTICIPANTS

Five right-handed participants were recruited for the experiments (mean age $\pm$ SD: 30.2 $\pm$ 3.4928). The experiment was approved by the Institute Ethics Committee of IIT Madras (Approval number: IEC/2020-03/SKM/02/10), and written consent of participation was taken from each participant before the start of the experiment. None of the participants had any history of neuromotor disorders or injuries to the hand and/or arms.

2) EXPERIMENTAL PROTOCOL

The participants were seated on a wooden chair throughout the experiment, and the right hand was rested on a wooden table near the participant. Care was taken to ensure that minimal metallic objects were in the vicinity of the experimental space to avoid electromagnetic interference in both the EMTS as well as the HKMS. For experiment 1, 16 EMTS microsensors were stuck to the right hand of the participants (15 on the finger phalanges and 1 on the wrist for reference) using double-sided tape at the sensor's bottom and surgical tape on the top. This ensured minimal movement of the sensor relative to its original position and orientation at the time of attachment. The EMTS source box was kept close to the right hand and served as the reference frame w.r.t which the sensors gave the orientation data.

The experiment was split into two tasks for each participant. In the first task, the participants were required to perform 26 hand postures derived from the American Sign Language (ASL) and Bharatanatyam postures (a classical Indian dance form) (See Fig. 4(a)). In the second task, the participants were required to grasp and release 10 different objects (See Fig. 4(a)). For each posture and object grasp, three trials of data were collected ($36 \times 3 = 108$ trials). A picture of the posture/object grasp that needed to be performed by the participant for a particular trial was displayed on a monitor kept in front of the participant. Each trial lasted for 8 seconds. At the start of each trial, the hand was kept flat on the table, with the fingers adducted and the palm facing downwards. This was the home position. At the 1s mark, the experimenter verbally indicated to the participant to perform the task as per the image on the screen and maintain the posture/object grasp. At the 6s mark, the participant was verbally indicated to return the hand back to the home position. The orientation data in the form of quaternions was collected for each trial from the EMTS sensors at an update rate of 100 Hz using a customized LabVIEW program. Experiment 2 was exactly the same as experiment 1, the only difference being that instead of using the EMTS to collect full hand kinematics data, the HKMS was used. Similar to experiment 1, a customized LabVIEW code was written to collect data from the HKMS at 100 Hz. All data analysis was performed using MATLAB.

3) CALIBRATION OF THE HKMS

For experiment 2, prior to the start of the experiment, all 16 BNO055 sensors of the HKMS were calibrated simultaneously. To do this, the HKMS was first mounted on the hand using double-sided tape. Then, the exact movements for calibrating a single BNO055 sensor were performed by the hand instead. This resulted in the simultaneous calibration of all the 16 BNO055 sensors. It should be mentioned that for the calibration of the gyroscopes, it was observed that when the participants kept their hand flat on the table and stiffened the joints in order to keep the hand stationary, the gyroscope did not get calibrated. Instead, when the hand was kept loose on the table without any effort to control the joints, the hand assumed a natural position and became motionless. In this state, the gyroscope of all the 16 sensors got calibrated immediately. The process to calibrate all the BNO055 sensors of the HKMS takes approximately 90s.

4) SENSOR TO SEGMENT ALIGNMENT

For the first experiment involving the EMTS sensors, the sensor-to-segment alignment was performed using the boresight function provided in the Polhemus proprietary software PiMgr. The hand was first aligned with the reference frame of the EMTS source box, and then the boresight function was executed. This function aligned all the sensor's reference frames via software with the source box's reference frame. Since the hand was aligned to the source box reference frame, the sensor reference frames now accurately represented the

orientation of the bones to which they were attached to post boresight. The boresight operation was done in two steps: 1. The four fingers and wrist were aligned to the source box reference frame, and all the attached sensors were boresighted. 2. The thumb was then aligned to the source box reference frame, and the thumb sensors were boresighted.

For the second experiment involving the BNO055, the sensor-to-segment alignment was done only for the sensors on the fingers. For the thumb sensors, the sensor-to-segment alignment was not required as the sensors were carefully attached along measured anatomical positions. The sensor-to-segment alignment for the finger sensors was done in the following way: for each trial, 50 samples (0.3 sec to 0.8 seconds, i.e., when the hand was at the home position) of the relative quaternions of each joint were averaged directly and renormalized. Such averaging produces minimum error since the data is static [29]. All the relative quaternions in the trial were then expressed w.r.t the averaged quaternion values to achieve sensor-to-segment alignment.

5) ROM AND STATIC RMSE COMPARISON

The ROM and RMSE of data from experiment 1 and 2 were computed and compared. First, the relative quaternions were computed between two adjacent joint segments for all joints. For ROM analysis, the relative quaternions were converted to Euler angles, and a box plot analysis was performed (separately for experiments 1 and 2) using data from all the participants. The ROM analysis was done to determine whether the HKMS could measure the maximum and minimum joint angle movement ranges for dexterous hand movements when compared to the EMTS sensors. For RMSE analysis, only data from the static part of the trials was considered for analysis. The 3.5s-4.5s interval was considered as the static part of the trial as the participants maintained the posture/object grasp with minimal changes in the joint angles during this interval. The RMSE for a posture/object grasp was computed in the following way: the relative quaternions of the 15 joints were averaged from the 3.5s to 4.5s interval to give 15 average quaternion values for a trial. This was done for all 3 trials of the posture and for all 5 participants, resulting in $15 \times 3 \times 5 = 225$ average quaternion values. These average quaternion values were computed for experiments 1 and 2, resulting in two datasets. The RMSE between the two datasets was calculated using (3) to yield the RMSE of the posture.

6) COMPARISON OF SYNERGIES

Studies in neuroscience through PCA (Principal Component Analysis) have demonstrated that a few control signals from the CNS can simultaneously activate a set of joints. This reduces the burden on the CNS to individually control each joint. It has been shown through eigenvector (also called synergy) analysis that the first few synergies explain more than 80% of the variance in data, and higher-order synergies reveal finer details of the posture [4]. Many of these studies were performed either using data gloves or optical trackers to compute joint angles. Since joint angles lie on a linear domain, PCA could be applied to it. However, IMU-based systems output orientation information in the form of quaternions or Euler angles which are defined along a non-linear manifold. Hence the direct application of PCA, which is a linear method, is not valid. To overcome this, the quaternions (from the HKMS and EMTS) were first linearized using logarithmic mapping and then PCA was applied to them [31]. The following are the steps involved in the analysis:

1. For each participant, hemispherized relative quaternions were arranged column-wise. Each joint had four data columns (referred to as a ''column block'') representing quaternion data. Since the relative quaternions for 15 joints were calculated, there were $15 \times 4 = 60$ columns of quaternion data (or 15 column blocks). For each participant, there were three trials for each of the 36 postures/object grasps and for each trial, data was collected at 100Hz for 8s. Hence, the total number of quaternion samples collected for a participant was 36 x 3 x 8 x 100 = 86400. This resulted in a data matrix of the dimension 86400 x 60.

2. The mean of each column block was computed using Markley's algorithm [36].

3. The quaternions in the column block were then calculated relative to the mean quaternion of that column block using (4). This step centered the data around zero.

$$q_{\text{centered}} = q_{\text{mean}}^{\ conj} \otimes q_{\text{sample}} \qquad (4)$$

4. Each of the 15 column blocks was then linearized using logarithmic mapping using equation (A1) (See Appendix – II). Such a mapping converts each of the 4 valued quaternions to 3 valued linear 3D vectors. This resulted in a data matrix of the dimension 86400×45.

5. Standard PCA using eigenvector decomposition was then applied on the linearized orientations.

The resulting eigenvectors or synergies computed from both the HKMS and the EMTS were compared using Pearson's correlation coefficient. The linearized eigenvectors were converted back to quaternions using exponential mapping (A2) to visualize the Eigen Postures. The details of the algorithm are provided in [31].

IV. RESULTS
A. JOINT ANGLE VALIDATION
1) STATIC VALIDATION

The results of the static validation are presented in Table 2. As can be seen from the table, the errors lie well within 2° for most of the options except for two options where the relative yaw angle was set at 45° and 60°. In these two options, the error was 2.91° and 3.54°, respectively. However, while performing hand postures, the yaw (abduction/adduction) angles are well within 60° (See Fig. 9); hence yaw errors as high as 3.54° are unlikely while performing static hand postures. Considering the entire data set of 120 trials, it was observed that there were some samples with absolute errors of up to 4° and one sample in which the error was 7.56°. However, these are outliers since the average values were less than 2° in most options. From this analysis, we conclude that the

TABLE 2. Statistics for static validation.

	Pitch	Yaw	Roll	Pitch	Yaw	Roll	Pitch	Yaw	Roll	Pitch	Yaw	Roll
Design 1– Pitch angles												
Actual (Set)	30	0	0	60	0	0	90	0	0	120	0	0
Maximum	32.5	1.63	1.26	60.5	1.7	2.9	92.98	0.8	3.76	123.04	3.58	3.86
Minimum	28.1	-1.5	-1.89	57.1	-3.7	-0.75	85.68	-2.0	-0.42	118.79	0.13	-2.09
Average	30.2	0.28	-0.11	58.9	-0.49	0.97	90.55	0.06	1.41	121.03	1.57	0.59
Error	0.2	0.28	0.11	1.1	0.49	0.97	0.55	0.06	1.41	1.03	1.57	0.59
Design 2– Roll angles												
Actual (Set)	0	0	30	0	0	60	0	0	90	0	0	120
Maximum	2.24	1.55	30.9	1.27	2.28	61.8	2.58	-0.05	93.1	3.69	0.23	122.4
Minimum	-0.49	-3.84	28.31	-1.65	-2.38	58.34	-1.55	-3.36	89.4	-2.67	-2.87	116.1
Average	0.26	-0.47	29.61	0.11	-0.18	59.94	0.75	-1.2	91.3	0.56	-0.96	119.54
Error	0.26	0.47	0.39	0.11	0.18	0.06	0.75	1.2	1.3	0.56	0.96	0.46
Design 3– Yaw angles												
Actual (Set)	0	15	0	0	30	0	0	45	0	0	60	0
Maximum	2.23	22.56	2.88	2.95	31.2	1.47	3.7	44.22	-0.1	2.35	59.19	4.98
Minimum	-0.015	14.44	-1.37	0.47	28.1	-2.45	-0.63	39.9	-4.42	-2.63	56.46	-0.77
Average	0.78	17.02	0.8	1.57	29.9	-0.2	1.12	42.09	-1.8	-0.42	57.57	2.5
Error	0.78	2.02	0.8	1.57	0.1	0.2	1.12	2.91	1.8	0.42	2.43	2.5

Colour coding used in the table: 4° >Error < 6°, Error > 6°. *All values in the above table are in degrees. Errors <4° are not highlighted*

BNO055 sensors have good static accuracy for the human hand movement range.

2) DYNAMIC VALIDATION

The RMSE between the relative quaternions of the BNO055 and the EMTS sensors for the different conditions and rotation speeds are presented in Fig 5.
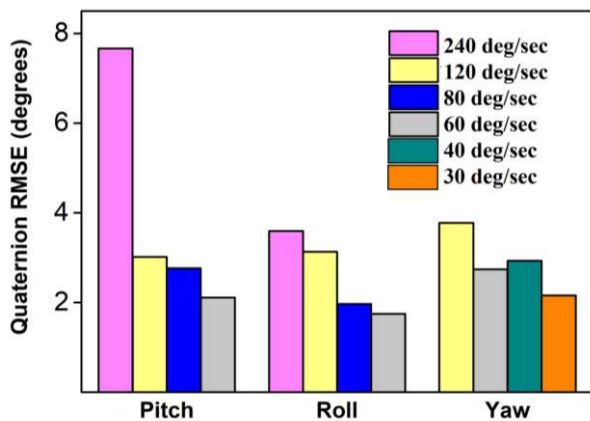

FIGURE 5. Quaternion RMSE computed for various rotation speeds. The rotation speeds for relative Yaw rotations are 120°/s, 60°/s, 40°/s and 30°/s. The rotation speeds for relative Pitch and Roll rotations are 240°/s, 120°/s, 80°/s and 60°/s.

As can be seen in the figure, except for the case of pitch rotation at 240°/s where the RMSE is 7.5°, the RMSE in all other cases are less than 4°. At the lowest rotation speeds for each of the three conditions, the RMSE values are around 2°. While RMSE provides information in the form of an average error, it is necessary to record the maximum error that occurred during the validation process. For this purpose, the angle between the two relative quaternions of the BNO055 and the EMTS sensors was computed using (5).

$$\theta = \left\| ln(Q_i^{conj} \otimes Q_e) \right\| \tag{5}$$

Here, Q_i and Q_e are the relative quaternions of the BNO055 and EMTS sensors, respectively. This angle is considered as the error and is the smallest angle required for one quaternion to rotate about an axis to reach the other quaternion. A box plot analysis of the error angles is presented in Fig. 6 for each of the three conditions. As can be seen from the plot, the median error is less than 4° for all the cases except for relative pitch rotations at 240°/s. Also, for rotation speeds of less than 240°/s, the maximum error lies within 10° for all three conditions. For the case of relative pitch movements at 240°/s, a maximum error of 25° is observed. Additionally, the number of outliers, in this case, are many.

To further investigate the high number of outliers and high RMSE error in the case of relative pitch rotation at 240°/s, a random trial was selected from each of the four-movement speeds for the relative pitch rotation condition. The relative pitch Euler angle from the selected trials was plotted for the BNO055 and EMTS sensors (See Fig. 7). From the figure, it can be seen that for rotation speeds of 60°/s, 80°/s and
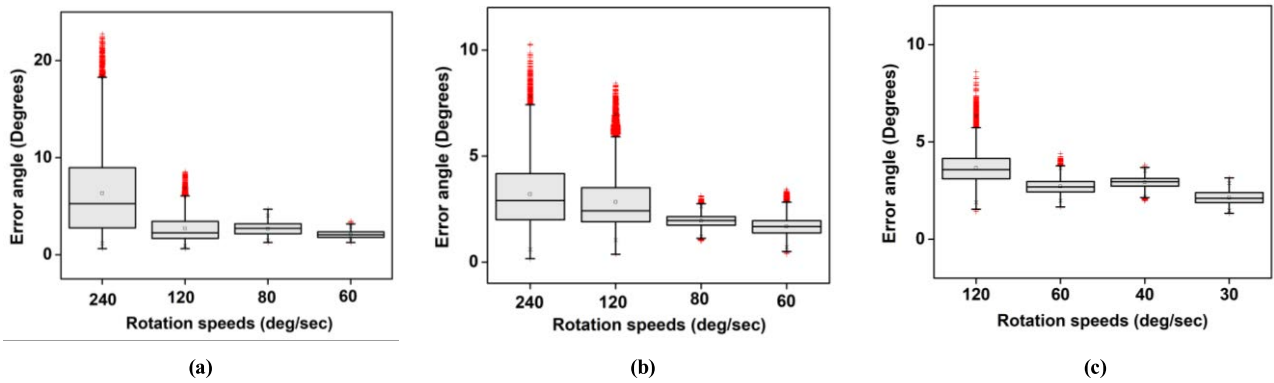
FIGURE 6. Box plots of the error angle for Pitch (a), Roll (b) and Yaw (c) rotations at various rotation speeds. The error angle is the angle between the relative quaternions of the BNO055 sensors and the EMTS sensors.
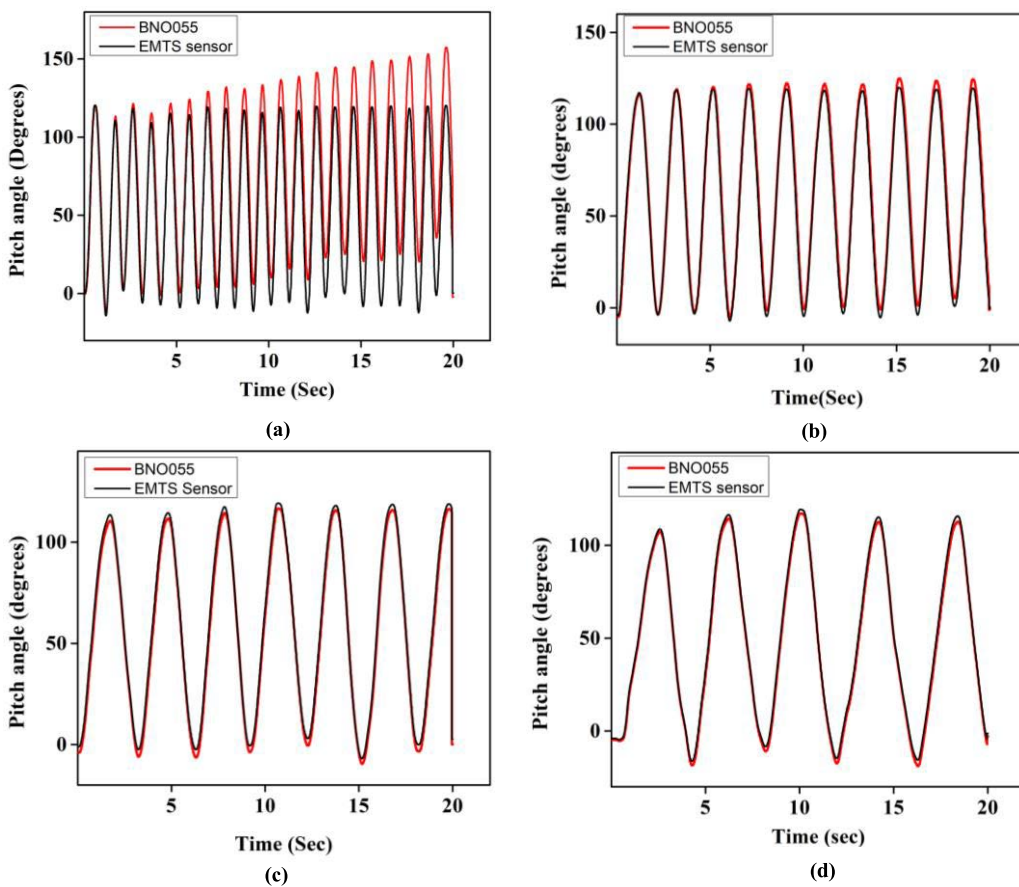

FIGURE 7. For relative pitch rotation (i.e., condition 3), the relative pitch Euler angle of the EMTS and BNO055 sensors are plotted for rotations speeds of (a) 240°/s, (b) 120°/s, (c) 80°/s and (d) 60°/s.

120°/s, the angles for both the BNO055 and EMTS sensors are almost the same, but for the rotation speed of 240°/s (See Fig. 7. (a)), the angle of the BNO055 starts to drift after the first few changes in the rotation direction. This results in an accumulation of error with time. The longer the movements are made continuously, the more is the magnitude of error, which explains the high number of outliers and the high RMSE. Furthermore, the error is more evident at the instance

of change in the direction of rotation (i.e., at the peaks and valleys) where there is a sudden change in the direction of acceleration. A possible explanation for errors at high rotation speeds can be found in the BNO055 datasheet, where it is mentioned that the BNO055s sensor fusion algorithm was designed for tracking human motion and that at high accelerations, the gravity vector may be misinterpreted as the high acceleration [32, p. 28]. If we consider human hand
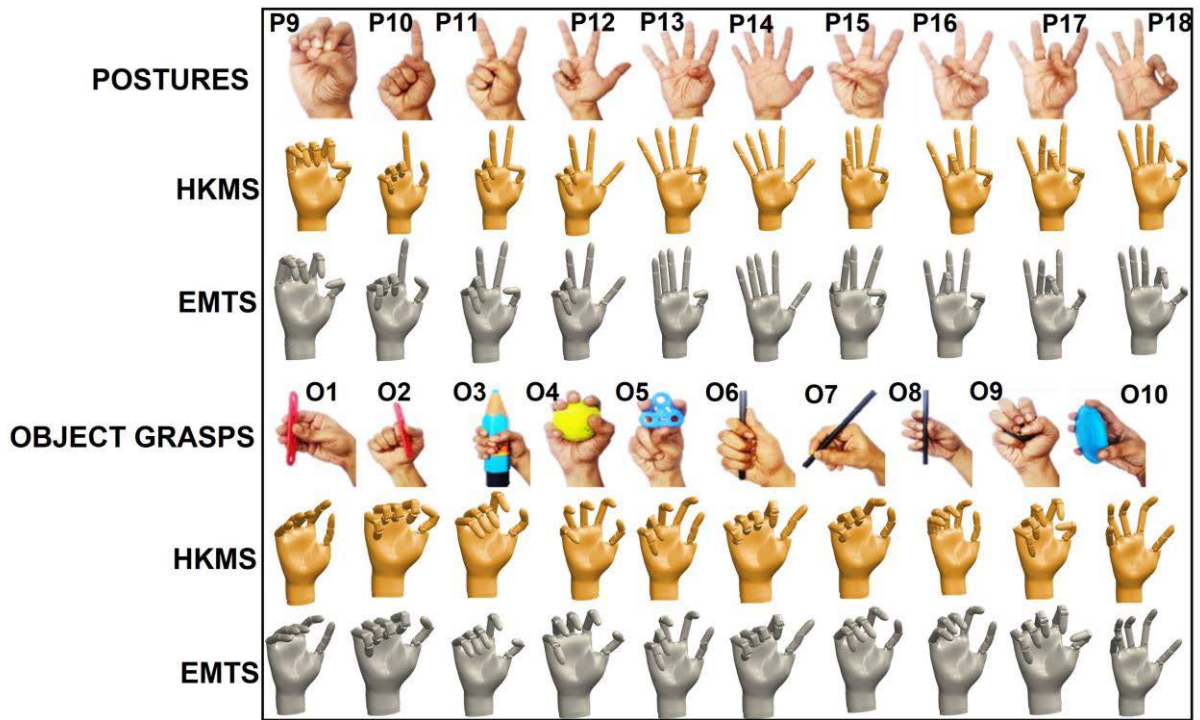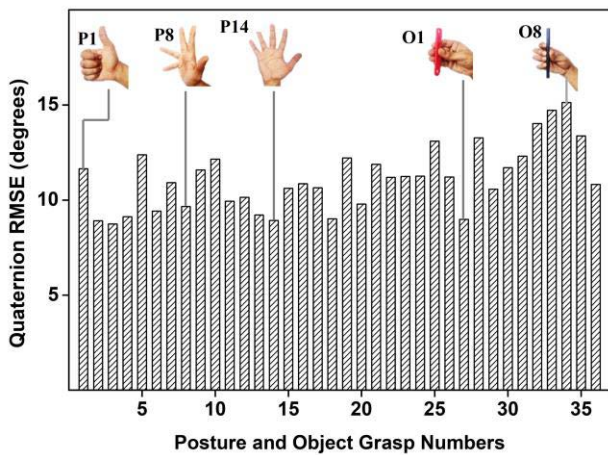
FIGURE 8. Images of ten hand postures and object grasps are generated for a randomly selected participant using data from experiment 1 (which was collected using EMTS) and experiment 2 (which was collected using HKMS) for the purpose of visual comparison. The hand model was created and rendered using SOLIDWORKS.
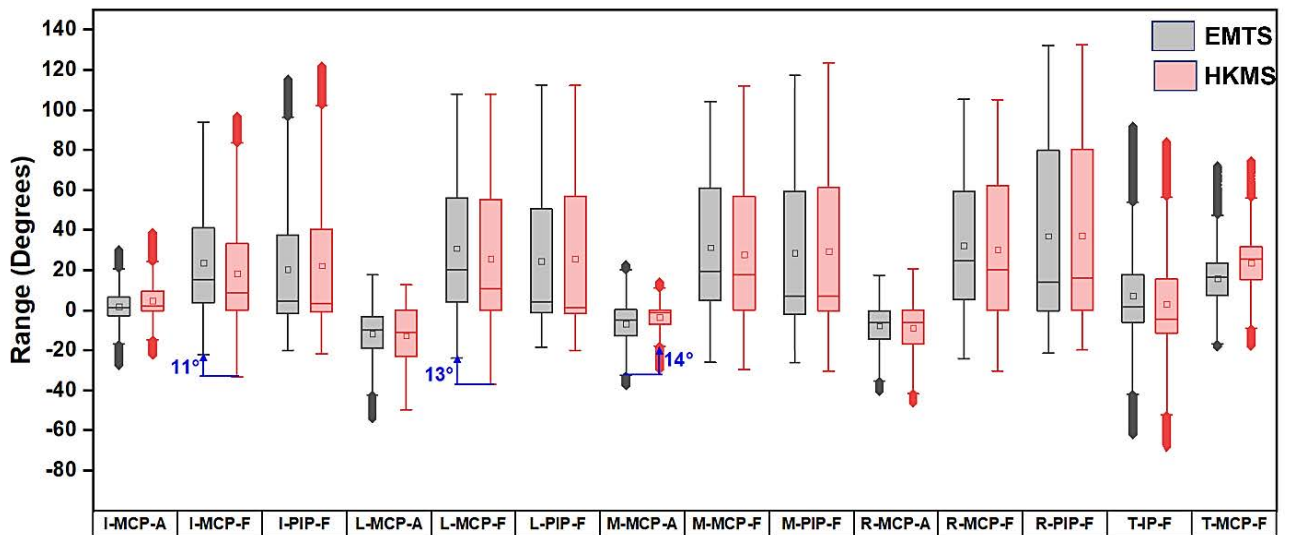

FIGURE 9. Box plots of various joint angles for experiments 1 (EMTS) and 2 (HKMS). Here the box plots for the metacarpophalangeal (MCP) joints and proximal interphalangeal (PIP) joints of the fingers and the MCP and interphalangeal (IP) joint of the thumb are presented for flexion/extension and abduction/adduction movements. I, L, M, R and T stand for index, middle, ring, little and thumb respectively and A and F stands for abduction and flexion respectively. I-MCP-A means the box plot is for the index MCP joint for abduction/adduction movements. Similarly, I-MCP-F means the box plot is for index MCP joint for flexion/extension movements. The top three maximum errors in measuring ROM between the HKMS and EMTS is highlighted in blue.

movements, repeated continuous rotations about a particular joint at high speeds (such as experienced by the BNO055 at the rotation speed of 240°/s) is unlikely. Furthermore, accumulation of error happens only for continuous

repeated movements. This can be seen in Fig. 7(a), where the angles start drifting only after the first four cycles of rotation. Hence, isolated high acceleration joint rotations in the human hand will not result in a high error. It should also

FIGURE 10. RMSE between the static postures/object grasps of experiment 1 (EMTS) and 2 (HKMS) are plotted. The images of some of the postures/object grasps are also shown in the figure. Maximum error is seen for postures and objects that involve more movement in the PIP or DIP joints.
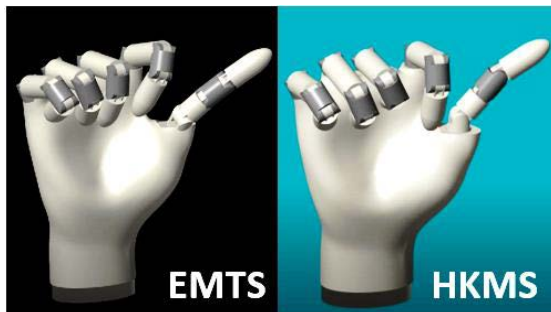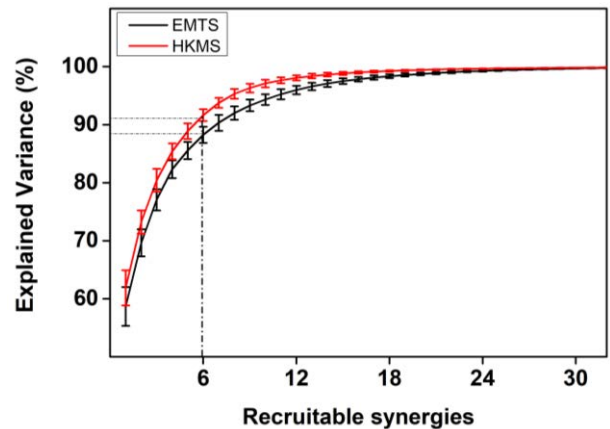

FIGURE 11. For a participant, a trial was randomly selected from experiment 1 (EMTS) and the static posture was generated. The corresponding trial from experiment 2 (HKMS) was used to generate another static posture. Upon visually comparing the two images, it can be seen that the differences between the two postures are in the finer details. Also, the flexion of the DIP joints is greater in the experiment 2 trial.

FIGURE 12. Scree plot for average percentage explained variance across participants vs synergies plotted for experiments 1 (EMTS) and 2 (HKMS).

FIGURE 13. Pearson's correlation coefficient computed between the kinematic synergy patterns of experiment 1 (EMTS) and experiment 2 (HKMS). The height of the bars indicates average correlation coefficient averaged across participants; the error bars indicate standard error of mean (SEM).
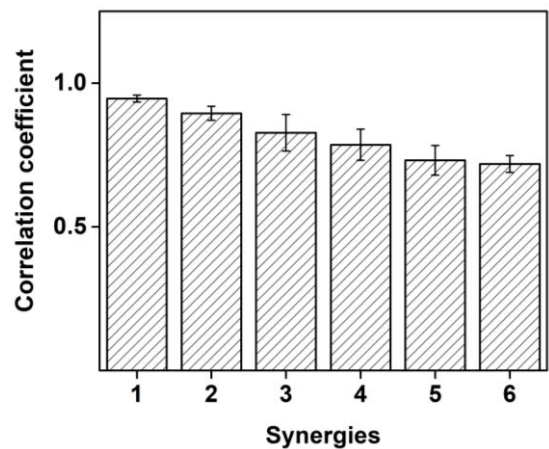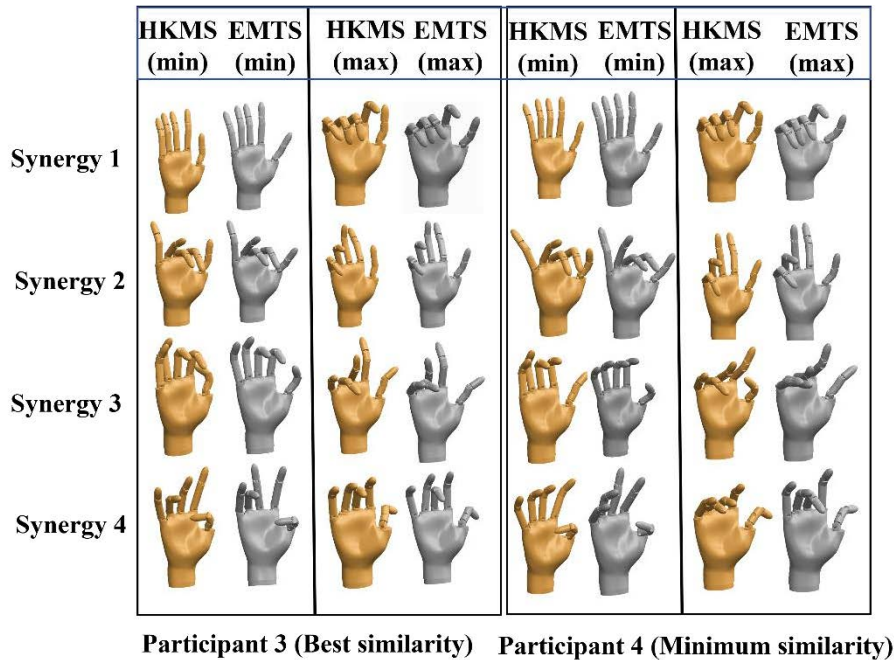
be noted that the data was collected in the presence of a magnetic field emitted from the EMTS source box. This could cause distortions in the magnetometer data of the BNO055 and affect its accuracy. Despite this fact, the RMSE values were found to be low except for relative pitch rotations at $240°/s$. From the above results and discussion, we conclude that the BNO055 sensors have acceptable dynamic accuracy for measuring human hand kinematics.

B. POSTURE VISUALIZATION IN 3D

A participant from experiment 1 and 2 was randomly selected, and the static hand postures/object grasps for that participant was generated. A few of these hand postures/object grasps are presented in Fig. 8. A visual examination of the images gives the impression that the postures/object grasps generated using the HKMS and EMTS are comparable. However, some observable differences can be attributed to the following reasons: 1. Since the images are generated

using two different experiments, there is variability in the posture/object grasp made by the participant itself. 2. During movement of the hand, the rigid wires of the EMTS sensors can cause movement in the sensors. Also, since the EMTS sensors are small and thin, they are prone to skin artifacts. In comparison, the BNO055 sensors have a flat surface and are less affected by skin artifacts and movements of the FFC cables. 3. The small EMTS sensor placed on the wrist is more affected by tendon movements than the flat BNO055 sensor placed on the wrist. This difference will be reflected in the overall posture generated using the EMTS and HKMS as the orientation of the finger's proximal phalanges and the thumb's metacarpal are calculated relative to the wrist sensor.

C. COMPARISON OF ROM AND STATIC RMSE

A box plot analysis of the joint angles from all participants of experiments 1 (EMTS) and 2 (HKMS) was done separately, as shown in Fig. 9. This plot was used to compare the ROM

HKMS EMTS (min) (min)	HKMS EMTS (max) (max)	HKMS EMTS (min) (min)	HKMS EMTS (max) (max)
Synergy 1			
Synergy 2			
Synergy 3			
Synergy 4			

Participant 3 (Best similarity)   **Participant 4 (Minimum similarity)**

FIGURE 14. Comparison of the first 4 Eigen postures computed using HKMS and EMTS separately for 2 participants- One for the participant for whom maximum similarity was observed between the EMTS and HKMS(Left), and the other for the participant who showed minimum similarity.

obtained from the HKMS and EMTS. For brevity, only the MCP and PIP joints for all the fingers and the MCP and IP joints of the thumb were compared. This is because the MCP and PIP joints exhibit higher ROMs and have higher movement velocities when compared to the DIP joint. Hence analyzing these joints is sufficient as any errors induced due to higher movement velocities will be seen at these joints. From Fig. 9, it can be seen that the ROMs computed using HKMS and EMTS are comparable. A maximum error of 11°, 13° and 14° was seen for the Index MCP joint flexion, little MCP joint flexion and middle MCP joint abduction/adduction, respectively. It should be noted that the maximum errors are observed at the MCP joints even though the PIP joints have similar movement ranges and angular velocities. A possible explanation for this, which is also mentioned in the preceding section, is that the wrist reference sensor of the EMTS and HKMS are affected differently by skin artifacts and tendon movements. This difference is manifested in the joint angles at the MCP joint, whose orientation is calculated relative to the wrist sensor. From this analysis and discussion, we conclude that the HKMS is reasonably accurate in calculating the ROM of the hand and could help clinicians to access the ROM for tracking the severity of pathology and recovery rate in patients with neuromotor disorders.

Additionally, the RMSE between the static postures/object grasps of the two experiments was computed. The results are presented in Fig. 10. The average static RMSE across all postures and object grasps is 11°, and the maximum and minimum RMSE values are 15° and 8°, respectively.

Considering the reasons mentioned in the preceding section for the differences in the images of the postures/object grasps generated using the HKMS and EMTS, these RMSE values represent the worst-case scenario. Additionally, the EMTS sensors were attached using bigger and stronger tapes to prevent their movement. This, coupled with the fact that the EMTS sensor wires are rigid, could perhaps have restricted the ROM of the hand when compared to the HKMS. In Fig. 11, it can be seen that the flexion of the DIP joints are less for the case of experiment 1 (EMTS). Considering all these points, the average RMSE value can be expected to be much lesser than 11°.

D. COMPARISON OF SYNERGIES
The synergies obtained by performing PCA on data from experiments 1 and 2 were tested for similarity using Pearson's correlation coefficient. The similarity test was performed separately for each participant. The scree plot for explained variance vs synergies is presented in Fig. 12. The figure shows that the first six synergies account for greater than 85% variance in the data for both the EMTS and HKMS. These six synergies were selected for comparison.

The synergies from both experiments were matched using a simple search and match algorithm. Such a mapping is necessary while comparing synergies because studies in the literature that have compared synergies for same postures from two different data sets have observed that synergies with large eigen values map one to one whereas synergies with low eigen values may not map one to one as they could

be invoked in different orders [3]. This could be due to differences in the finer details of the postures that prevails between the two datasets. Hence, methods like the greedy search algorithm [33] and clustering analysis [5] have been employed to group similar synergies across datasets.

In this study, a greedy search algorithm was employed, where the first synergy from experiment 1 for a participant was compared with all other synergies from experiment 2 for maximum correlation using the absolute value of Pearson's correlation coefficient. Once a matching synergy was obtained, that pair was removed, and the next synergy from experiment 1 was matched similarly with one of the remaining synergies of experiment 2. This process was repeated until all synergy pairs were obtained. The p-values for every computed correlation coefficient were recorded. The p-values for all individual correlation coefficients showed that the correlations were significant ($p < 0.001$). The correlation coefficients for each synergy were then averaged across all participants and the results are presented in Fig. 13. The plot shows that the first two synergies (which represent gross movements) are very similar, with an average correlation coefficient of 0.94 ± 0.01198 (mean $\pm$ SEM) and 0.89 ± 0.0243 for the first and second synergies, respectively. Higher-order synergies (which represent finer movements) are reasonably similar, with average correlation coefficients for the 6th synergy (one with the lowest similarity compared to other synergies) being 0.72 ± 0.029. This result aligns with the observations we made in the preceding sections, where the overall postures/object grasps between experiments 1 and 2 visually looked similar, and the differences were observed only in the finer details.

To visualize the Eigen postures, the synergies were rotated in either direction from the mean posture to obtain the maximum and minimum range of Eigen postures. These Eigen posture ranges were computed using:

$$Eigen\ Posture_{max} = qs_i \otimes q\mu_i \tag{6}$$

$$Eigen\ Posture_{min} = qs_i^{conj} \otimes q\mu_i \tag{7}$$

where qs_i is the ith synergy, and $q\mu_i$ is the mean posture.

The resulting Eigen postures for experiments 1 and 2 are depicted in Fig. 14 for two participants- one for whom the best similarity was observed (participant 3) and the other for whom the similarity was minimum (participant 4). Visually, minimal differences can be seen between the postures of experiments 1 and 2 for the participant whose synergies were similar. For the other participant, except for the flexion of a few of the joints in the third and fourth synergy, the other synergies visually looked to be mostly similar.

V. CONCLUSION

This paper presents the design, validation, and application of a novel BNO055 IMU-based full Hand Kinematic Measurement System (HKMS). The HKMS outputs orientation data from 16 IMU sensors in real-time at 100 Hz. In contrast, many of the existing IMU based data gloves output data at lower sampling rates (e.g., 20 Hz [11], 50 Hz [17], [18], [20], [23], [25], 60 Hz [21] etc.,) while some IMU based data gloves have lesser number of IMU sensors [12], [17]. Furthermore, the HKMS uses Wi-Fi for wireless data transmission. Some of the IMU gloves use USB as the mode of data transmission [11], [12], [16], [24]. This limits the movement range of the glove to the length of the USB cable. IMU gloves that use Bluetooth [17], [18], [20], [21], [22], [23], [25] for wireless data transmission overcome this limitation. The advantage of using Wi-Fi in the HKMS over Bluetooth is that it provides superior range and data transmission speeds. Another advantage of the HKMS is that the number of BNO055 sensors can be increased from 16 to 20 without affecting the 100 Hz data output rate. These additional sensors can be placed on the wrist to model the palm arch of the hand or on the arms to capture their movement kinematics. Furthermore, studies that present an application [19] of the developed IMU data glove in a laboratory or clinical setup are scarce. In this paper, as an application of the HKMS, we have collected hand kinematic data for an experiment using the HKMS and performed synergy analysis on the dataset. Finally, the HKMS can be reproduced by those people who do not necessarily have an intimate knowledge of signal processing techniques and complex filters which are required for implementing the sensor fusion algorithm in real-time. This is because the HKMS uses the BNO055 IMU which implements its own sensor fusion algorithm (using an on-board microcontroller as part of the IMU chip) to directly output orientation data in the form of quaternions and Euler angles.

A rigorous static and dynamic validation of the BNO055 sensor was done to determine whether it is accurate enough to collect hand kinematic data in a clinical or laboratory setting. For the dynamic validation, continuous back and forth relative rotations between two BNO055s at different speeds were investigated. IMU based data glove studies in the literature that have done a similar dynamic validation are scarce. It was found that the RMSE error was less than 4° in all cases of static and dynamic validation except for the dynamic validation case of pitch rotation at 240°/s, where the RMSE error was 7.5°. Upon further analysis of this case, it was found that error was not present during the first few rotation cycles during any trial. As the movements were made continuously during a trial, the error accumulated and increased with time. This error can be attributed to the fact that the BNO055s sensor fusion algorithm was designed for tracking human movements where continuous high rotation speeds about a joint are unlikely. Furthermore, isolated high acceleration joint rotations will not result in an error as the error is observed only during continuous rotations after the first few rotation cycles. Keeping these points in mind, we conclude that the BNO055 can be used to collect hand kinematic data with reasonable accuracy.

To test the HKMS as a whole, its performance was juxtaposed with the performance of the highly accurate EMTS. To do this, two identical experiments were conducted where
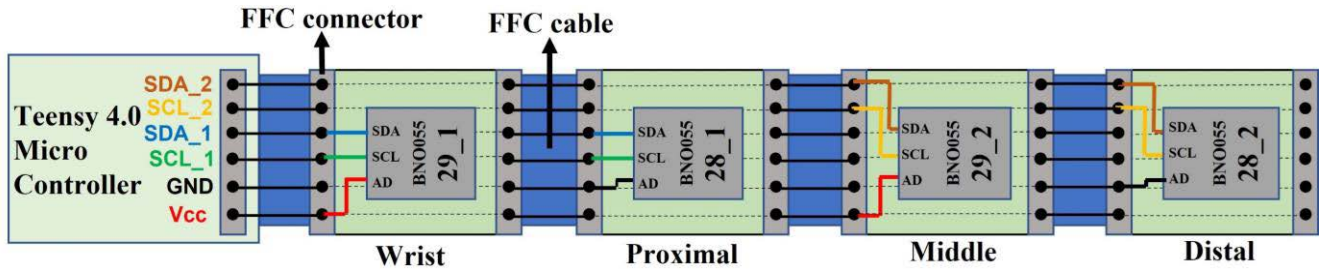
FIGURE 15. Simplified connections of a teensy microcontroller to four different types of custom PCB's designed around the BNO055 chip. These four types of PCB's are named: 29_1, 28_1, 29_2 and 28_2. Two BNO055 chips are connected to I2C channel 1 (28_1 and 29_1) and the other two are connected to I2C channel 2 (28_2 and 29_2) of the teensy. The address of the BNO055 chip is either set to 0×28 or 0×29, depending on the voltage connected to its address pin (AD). SCL_1 and SDA_1 together form I2C channel 1. Similarly, SCL_2 and SDA_2 form I2C channel 2.

the participants performed hand postures and object grasps. For one experiment, the EMTS was used to collect hand kinematic data, whereas the HKMS was used for the other experiment. The experiment protocol and participants were the same in both the experiments and the validation was done by comparing the two datasets. The average RMSE between the static postures derived from the two data sets was found to be 11°. The ROMs using the two datasets were calculated, and the errors were computed. A maximum ROM error of 14° was observed at one of the joints; all other errors were below this. The RMSE of the static postures and ROM errors represent the worst-case scenario, and actual errors can be expected to be much lesser. This is due to the following facts: 1. There was variability in the postures generated by the participants for the two experiments. 2. Skin artifacts and tendon movements affected the EMTS sensors and the BNO055 IMUs differently, especially the reference sensor on the wrist. 3. The rigid wires of the EMTS sensors restricted the ROM of the hand. Finally, synergy analysis was done on the two datasets, and it was demonstrated through the strength of correlation coefficients between the synergies computed from the two data sets that the HKMS could be successfully used to conduct synergy-based studies.

The limitation with the approach of validating the HKMS as a whole was that data from the HKMS and EMTS was not collected simultaneously from the participants in a single experiment. This was because the BNO055 IMU's and the EMTS microsensors could not be mounted together on the finger phalanges due to lack of space on the phalanges. Alternatively, the gold standard stereophotogrammetric system can be used for validating the HKMS as a whole. This is because the small markers used in such systems can be mounted on top of the IMU sensors [16], [17]. Utility of such systems for validation of IMU's have also been demonstrated in other applications like measurement of body COM [34]. This would enable simultaneous collection of data from both the systems. Such a validation method is desired and can be taken up as part of the future work. In conclusion, the accuracy of two individual BNO055 sensors in calculating joint angles yielded good results (both for the static and dynamic conditions) and the validation of the HKMS as a

whole yielded promising results despite some limitations in the validation method. Keeping these points in mind, we are cautiously optimistic in suggesting the usage of the developed HKMS device in collecting hand kinematic data in research and clinical setups.

APPENDIX I
DESIGN FOR CONNECTING THE BNO055's IN SERIES

To connect the BNO055 sensors in series, four different "types" of custom PCBs were designed. Before describing the design of these four types of PCBs, a brief description of the I2C communication protocol is presented. The I2C protocol is used for serial communication with the BNO055 sensors. This protocol requires two lines for communication – SCL (Serial Clock) and SDA (Serial Data). The SCL and SDA lines together form a single I2C channel. Each I2C compatible device has an address using which it is communicated with. Hence, multiple I2C compatible devices can be connected on the same I2C channel and can be communicated with using their unique address. The BNO055 sensors can be assigned only two addresses for I2C communication: 0×28 and 0×29 (hexadecimal number notation). The BNO055 chip contains an address pin using which one of the two addresses can be set for the chip. The address is set to 0×29 or 0×28 if the address pin is connected to Vcc (3.3V) or GND (0V), respectively.

Since only two unique addresses can be assigned to the BNO055, only two BNO055 sensors can be connected to a single I2C channel. Our requirement was to connect at most four sensors in series. To achieve this, two I2C channels on each teensy were used, and four different types of custom PCB boards were designed around the BNO055 chip. These boards were named as: 29_1, 28_1, 29_2 and 28_2 (See Fig. 15). The naming convention is as follows: "chip address_I2C channel". For e.g., 28_1 means that the BNO055 chip's address is 0×28, and its I2C pins are connected to the I2C channel 1 of the teensy. Each BNO055 PCB has two 6 pin FFC connectors at its two ends (See Fig. 15) soldered at the bottom of the custom PCB. The 6 pins of the FFC connector are connected to Vcc, GND and the two I2C channels (2 pins per channel) of the teensy. The

pins on both the FFC connectors are connected to each other (See dotted lines in Fig. 15). This will allow for two FFC cables to be connected at its two ends hence enabling multiple sensors to be connected in series. The only difference in the four PCB types are the connections from the FFC pins to the SCL, SDA and AD (address) pins of the BNO055 chip. For 29_1 and 28_1 PCBs, the connections to the BNO055s I2C pins (SCL and SDA) are from I2C channel 1, and the connections to the address pin are Vcc and GND, respectively. However, for 29_2 and 28_2 PCBs, the connections to the BNO055s I2C pins are from I2C channel 2, and the connections given to the address pin are Vcc and GND, respectively (See Fig. 15). Such an arrangement allows for four BNO055s to be connected in series (two BNO055s each on I2C channels 1 and 2) and eliminates the need to have individual FFC cables and connectors connecting each BNO055 sensor to the Master-Slave PCB. This reduces the bulkiness of the device. The remaining connections and components on the four types of custom PCB (not discussed or shown in this paper) are the same and are as per the latest BNO055 manual [32].

APPENDIX II
LOGARITHMIC MAPS AND EXPONENTIAL MAPS

All formats of joint angle representation like Rotation matrix, Euler angles and quaternions are defined in the nonlinear domain and linear operations like averaging, linear dimensionality reduction etc., are not valid [31]. In cases where linear operations are required, one could linearize the quaternions using logarithmic mapping (A1). A quaternion of the form $q = (q_w, q_v)$ can be linearized by taking a log of the quaternion. Such a map, takes the quaternion from a 4D hypersphere to a 3D plane defined at unity [30]. In equation A1, since the quaternion is a unit quaternion, $ln |q| = 0$, we obtain a 3-element tuple $v = [v_x, v_y, v_z]$, which encodes information of both the angle and axis.

$$\ln q = \left(ln |q|, \left(\frac{1}{\|q_v\|} arccos \frac{q_w}{|q|} \right) q_v \right) \qquad (A1)$$

The new entity is a 3D vector, and all linear operations are valid on this vector. After applying linear operations, the vectors are mapped back to the hypersphere by taking an exponent of the vector (equation A2). Such a map is called as an exponential map.

$$q = e^v = \left[cos \left(\frac{\theta}{2} \right), sin \left(\frac{\theta}{2} \right) \frac{v}{\|v\|} \right] \qquad (A2)$$

where $\theta = \|v\|$

However, such transformations will incur a singularity which causes a sudden jump in values if the angle between any 2 vectors approaches 2π radians [30]. Since we deal with only relative quaternions and relative angles between any 2 phalanges are very small and never approaches 2π radians, the conversion to and from the exponential map is free of any singularity. The Matlab function 'quatlog' for logarithmic maps and 'quatexp' for exponential maps were utilized in this study.

REFERENCES

[1] C. D. Santina, M. Bianchi, G. Averta, S. Ciotti, V. Arapi, S. Fani, E. Battaglia, M. G. Catalano, M. Santello, and A. Bicchi, "Postural hand synergies during environmental constraint exploitation," *Frontiers Neurorobot.*, vol. 11, p. 41, Aug. 2017.

[2] C. R. Mason, J. E. Gomez, and T. J. Ebner, "Hand synergies during reach-to-grasp," *J. Neurophysiol.*, vol. 86, no. 6, pp. 2896–2910, Dec. 2001.

[3] P. H. Thakur, A. J. Bastian, and S. S. Hsiao, "Multidigit movement synergies of the human hand in an unconstrained haptic exploration task," *J. Neurosci.*, vol. 28, no. 6, pp. 1271–1281, Feb. 2008.

[4] M. Santello, M. Flanders, and J. F. Soechting, "Postural hand synergies for tool use," *J. Neurosci.*, vol. 18, no. 23, pp. 10105–10115, Dec. 1998.

[5] N. J. Jarque-Bou, A. Scano, M. Atzori, and H. Müller, "Kinematic synergies of hand grasps: A comprehensive study on a large publicly available dataset," *J. NeuroEng. Rehabil.*, vol. 16, no. 1, Dec. 2019.

[6] N. Jarrassé, A. Ribeiro, A. Sahbani, W. Bachta, and A. Roby-Brami, "Analysis of hand synergies in healthy subjects during bimanual manipulation of various objects," *J. NeuroEng. Rehabil.*, vol. 11, no. 1, p. 113, 2014.

[7] R. Vinjamuri, M. Sun, C.-C. Chang, H.-N. Lee, R. J. Sclabassi, and Z.-H. Mao, "Temporal postural synergies of the hand in rapid grasping tasks," *IEEE Trans. Inf. Technol. Biomed.*, vol. 14, no. 4, pp. 986–994, Jul. 2010.

[8] A. A. Portnova-Fahreeva, F. Rizzoglio, I. Nisky, M. Casadio, F. A. Mussa-Ivaldi, and E. Rombokas, "Linear and non-linear dimensionality-reduction techniques on full hand kinematics," *Frontiers Bioeng. Biotechnol.*, vol. 8, p. 429, May 2020.

[9] J. Zhou, F. Malric, and S. Shirmohammadi, "A new hand-measurement method to simplify calibration in CyberGlove-based virtual rehabilitation," *IEEE Trans. Instrum. Meas.*, vol. 59, no. 10, pp. 2496–2504, Oct. 2010.

[10] A. Roda-Sales, J. L. Sancho-Bru, M. Vergara, V. Gracia-Ibáñez, and N. J. Jarque-Bou, "Effect on manual skills of wearing instrumented gloves during manipulation," *J. Biomechanics*, vol. 98, Jan. 2020, Art. no. 109512.

[11] H. Liu, X. Xie, M. Millar, M. Edmonds, F. Gao, Y. Zhu, V. J. Santos, B. Rothrock, and S.-C. Zhu, "A glove-based system for studying hand-object manipulation via joint pose and force sensing," in *Proc. IEEE/RSJ Int. Conf. Intell. Robots Syst. (IROS)*, Sep. 2017, pp. 6617–6624.

[12] F. Fei, S. Xian, X. Xie, C. Wu, D. Yang, K. Yin, and G. Zhang, "Development of a wearable glove system with multiple sensors for hand kinematics assessment," *Micromachines*, vol. 12, no. 4, p. 362, Mar. 2021.

[13] A. Mohan, G. Tharion, R. K. Kumar, and S. R. Devasahayam, "An instrumented glove for monitoring hand function," *Rev. Sci. Instrum.*, vol. 89, no. 10, Oct. 2018, Art. no. 105001.

[14] J. Malešević, M. Kostić, V. Kojić, O. Dordević, L. Konstantinović, T. Keller, and M. Štrbac, "BEAGLE—A kinematic sensory system for objective hand function assessment in technology-mediated rehabilitation," *IEEE Trans. Neural Syst. Rehabil. Eng.*, vol. 29, pp. 1817–1826, 2021.

[15] Z. Lin, Y. Xiong, H. Dai, and X. Xia, "An experimental performance evaluation of the orientation accuracy of four nine-axis MEMS motion sensors," in *Proc. 5th Int. Conf. Enterprise Syst. (ES)*, Sep. 2017, pp. 185–189.

[16] H. G. Kortier, V. I. Sluiter, D. Roetenberg, and P. H. Veltink, "Assessment of hand kinematics using inertial and magnetic sensors," *J. NeuroEng. Rehabil.*, vol. 11, no. 1, p. 70, 2014.

[17] T. L. Baldi, S. Scheggi, L. Meli, M. Mohammadi, and D. Prattichizzo, "GESTO: A glove for enhanced sensing and touching based on inertial and magnetic sensors for hand tracking and cutaneous feedback," *IEEE Trans. Human-Mach. Syst.*, vol. 47, no. 6, pp. 1066–1076, Dec. 2017.

[18] B. Fang, F. Sun, H. Liu, and D. Guo, "Development of a wearable device for motion capturing based on magnetic and inertial measurement units," *Sci. Program.*, vol. 2017, pp. 1–11, Jan. 2017.

[19] J. Connolly, J. Condell, B. O'Flynn, J. T. Sanchez, and P. Gardiner, "IMU sensor-based electronic goniometric glove for clinical finger movement analysis," *IEEE Sensors J.*, vol. 18, no. 3, pp. 1273–1281, Nov. 2017.

[20] B.-S. Lin, I.-J. Lee, S.-Y. Yang, Y.-C. Lo, J. Lee, and J.-L. Chen, "Design of an inertial-sensor-based data glove for hand function evaluation," *Sensors*, vol. 18, no. 5, p. 1545, May 2018.

[21] Y. Choi, K. Yoo, S. J. Kang, B. Seo, and S. K. Kim, "Development of a low-cost wearable sensing glove with multiple inertial sensors and a light and fast orientation estimation algorithm," *J. Supercomput.*, vol. 74, no. 8, pp. 3639–3652, Aug. 2018.

[22] C. Salchow-Hömmen, L. Callies, D. Laidig, M. Valtin, T. Schauer, and T. Seel, "A tangible solution for hand motion tracking in clinical applications," *Sensors*, vol. 19, no. 1, p. 208, Jan. 2019.

[23] B.-S. Lin, I.-J. Lee, P.-Y. Chiang, S.-Y. Huang, and C.-W. Peng, "A modular data glove system for finger and hand motion capture based on inertial sensors," *J. Med. Biol. Eng.*, vol. 39, no. 4, pp. 532–540, Aug. 2019.

[24] H.-T. Chang and J.-Y. Chang, "Sensor glove based on novel inertial sensor fusion control algorithm for 3-D real-time hand gestures measurements," *IEEE Trans. Ind. Electron.*, vol. 67, no. 1, pp. 658–666, Jan. 2020.

[25] B.-S. Lin, I.-J. Lee, and J.-L. Chen, "Novel assembled sensorized glove platform for comprehensive hand function assessment by using inertial sensors and force sensing resistors," *IEEE Sensors J.*, vol. 20, no. 6, pp. 3379–3389, Mar. 2020.

[26] V. Patel, J. Craig, M. Schumacher, M. K. Burns, I. Florescu, and R. Vinjamuri, "Synergy repetition training versus task repetition training in acquiring new skill," *Frontiers Bioeng. Biotechnol.*, vol. 5, p. 9, Feb. 2017.

[27] W. Chen, C. Xiong, and S. Yue, "Mechanical implementation of kinematic synergy for continual grasping generation of anthropomorphic hand," *IEEE/ASME Trans. Mechatronics*, vol. 20, no. 3, pp. 1249–1263, Jun. 2015.

[28] M. K. Burns, K. Van Orden, V. Patel, and R. Vinjamuri, "Towards a wearable hand exoskeleton with embedded synergies," in *Proc. 39th Annu. Int. Conf. IEEE Eng. Med. Biol. Soc. (EMBC)*, Jul. 2017, pp. 213–216.

[29] J. H. Challis, "Quaternions as a solution to determining the angular kinematics of human movement," *BMC Biomed. Eng.*, vol. 2, no. 1, pp. 1–10, Dec. 2020.

[30] F. S. Grassia, "Practical parameterization of rotations using the exponential map," *J. Graph. Tools*, vol. 3, no. 3, pp. 29–48, Jan. 1998.

[31] M. P. Johnson, "Exploiting quaternions to support expressive interactive character motion," Ph.D. dissertation, Dept. Media, Arts Sci., Massachusetts Inst. Technol., Cambridge, MA, USA, 2003.

[32] *BNO055 Intelligent 9-Axis Absolute Orientation Sensor, Revision 1.8*, document BNO055 datasheet, Bosch Sensortec, Kusterdingen, Germany, Nov. 2014.

[33] D. Liang, M. Yarossi, S. L. Jacobs-Skolik, M. P. Furmanek, D. Brooks, D. Erdogmus, and E. Tunik, "Synergistic activation patterns of hand muscles in left-and right-hand dominant individuals," *J. Hum. Kinetics*, vol. 76, no. 1, pp. 89–100, Jan. 2021.

[34] S. Cardarelli, A. Mengarelli, A. Tigrini, A. Strazza, F. Di Nardo, S. Fioretti, and F. Verdini, "Single IMU displacement and orientation estimation of human center of mass: A magnetometer-free approach," *IEEE Trans. Instrum. Meas.*, vol. 69, no. 8, pp. 5629–5639, Aug. 2020.

[35] Bosch Sensortec. (Dec. 20, 2016). *Bosch Sensortec Tutorials: How to Calibrate the Absolute Orientation Sensor BNO055*. Accessed: Apr. 8, 2022. [Online]. Available: https://www.youtube.com/watch?v=Bw0WuAyGsnY

[36] F. L. Markley, Y. Cheng, J. L. Crassidis, and Y. Oshman, "Averaging quaternions," *J. Guid., Control, Dyn.*, vol. 30, no. 4, pp. 1193–1197, Jul. 2007.

PRAJWAL SHENOY received the B.Tech. and M.Tech. degrees in mechanical engineering. He is currently pursuing the Ph.D. degree in biomedical engineering with the Department of Applied Mechanics, Indian Institute of Technology, Madras, India. He is an Assistant Professor with the Department of Mechatronics Engineering, Manipal Institute of Technology, MAHE, Manipal. His research interests include analysis of human hand kinematics and application of computational techniques in analysis of human hand movements.

ANURAG GUPTA received the B.Tech. degree in biomedical engineering from the Manipal Institute of Technology, Manipal. He is currently pursuing the M.Tech. and Ph.D. dual degrees in biomedical engineering with the Department of Applied Mechanics, Indian Institute of Technology, Madras, India. His research interest includes motor control. He is interested in behavioral studies involving the human hand and device development to measure human hand kinematics.

VARADHAN S.K.M. received the Ph.D. degree in kinesiology from Pennsylvania State University, PA, USA. He is an Associate Professor with the Biomedical Engineering Group, Department of Applied Mechanics, Indian Institute of Technology, Madras, India. His research interests include motor control, use of experimental and computational techniques in understanding neural control of movement, application of engineering in rehabilitation, and applications of noninvasive techniques in biomedical movement analysis.

• • •